Catalysis Today xxx (2016) xxx–xxx

Contents lists available at ScienceDirect

Catalysis Today

journal homepage: www.elsevier.com/locate/cattod

CO and CO_2 methanation over supported Ni catalysts

Thien An Le, Min Sik Kim, Sae Ha Lee, Tae Wook Kim, Eun Duck Park*

Department of Chemical Engineering and Department of Energy Systems Research, Ajou University, 206, World Cup-Ro, Yeongtong-Gu, Suwon 16499, Republic of Korea

ARTICLE INFO

Article history:
Received 1 September 2016
Received in revised form
26 November 2016
Accepted 16 December 2016
Available online xxx

Keywords:
CO Methanation
CO_2 Methanation
Ni catalyst
Support effect
CeO_2

ABSTRACT

CO and CO_2 methanation was investigated over Ni catalysts supported on different supports such as γ-Al_2O_3, SiO_2, TiO_2, CeO_2, and ZrO_2. Among them, Ni/CeO_2 was determined to be the most active for CO and CO_2 methanation. These catalytic activities increased with increasing surface area of CeO_2. To increase the specific catalytic activity for CO and CO_2 methanation, various Ni-CeO_2 catalysts with different Ni contents were prepared using co-precipitation method. The optimum Ni content was determined for both reactions. The prepared catalysts were characterized with inductively coupled plasma-atomic emission spectroscopy, N_2 physisorption, temperature-programmed reduction, temperature-programmed desorption, and X-ray diffraction. The high Ni dispersion and strong CO_2 adsorption appeared to be responsible for the high catalytic activity for CO and CO_2 methanation. This Ni-CeO_2 can be applied to the low-temperature CO and CO_2 methanation reactor to achieve high single-pass conversions of CO and CO_2.

1. Introduction

Methane, which can be found as a main component in natural gas and shale gas, is one of important energy resources and chemical feedstocks. Therefore, the infrastructure for its delivery has been well developed and equipped throughout the nations. This enables us to use methane as an energy carrier now and future.

Although methane can be found in nature, a synthetic natural gas has been commercially produced from different starting materials including coal and biomass. In this process, syngas (a mixture of CO and H_2) is transformed into methane through CO methanation, as follows:

$$CO(g) + 3H_2(g) \leftrightarrow CH_4(g) + H_2O(g); \triangle H^\circ_{298K} = -206\,kJ\,mol^{-1} \quad (1)$$

This reaction is also used in the purification process in hydrogen and ammonia production plants [1]. Recently, selective CO methanation in the presence of an excessive amount of CO_2 has been intensively studied to remove residual CO from the reformed gas for the polymer electrolyte membrane fuel cells [2].

Besides CO methanation, a synthetic natural gas can be produced from CO_2 through CO_2 methanation, as follows:

$$CO_2(g) + 4H_2(g) \leftrightarrow CH_4(g) + 2H_2O(g); \triangle H^\circ_{298K} = -165\,kJ\,mol^{-1} \quad (2)$$

This is a rather simple chemical route among a variety of catalytic CO_2 hydrogenation techniques [3,4]. Together with H_2 production by water electrolysis, this consists of the Power-to-Gas technology which connects the power grid with the gas grid by transforming surplus power into a grid compatible gas [5].

Since Sabatier and Senderens first reported this reaction in 1902 [6], a number of works have been conducted for this reaction [7–12]. Vannice [7] compared the catalytic activity for CO methanation over various transition metals and found that the order of decreasing activity was Ru > Fe > Ni > Co > Rh > Pd > Pt, Ir. Owing to its high activity and relatively cheap price, nickel has been selected as an active metal for CO and CO_2 methanation. Besides active metal, a support plays a critical role in the catalysis by stabilizing the active site as well as enhancing the adsorption of key reactants. Until now, lots of supports including γ-Al_2O_3 [13], barium hexaaluminate [14], SiO_2 [13], MCM-41[15], *meso*-structured silica nanoparticles (MSN) [15], SiC [16], HY [15], 5A zeolite [17], TiO_2 [13], calcium titanate [18], ZrO_2 [13], CeO_2 [19–24], ceria–zirconia binary oxide [25], Metal–organic frameworks (MOFs) [26], and carbon nanofiber (CNF) [27] have been utilized for supported Ni catalysts. However, only a few works have been disclosed on the comparative study for CO or CO_2 methanation over Ni catalysts supported on different supports under same reaction conditions. Takenaka et al. [13] compared the catalytic activity for CO methanation over supported Ni catalysts and claimed that ZrO_2 was the best support among γ-Al_2O_3, SiO_2, TiO_2, and ZrO_2. Zhen et al. [15] reported that the activity of CO_2 methanation followed an order of Ni/MSN > Ni/MCM–41 > Ni/HY > Ni/SiO_2 > Ni/γ-Al_2O_3.

In this work, we carried out the comparative study for CO and CO_2 methanation over Ni catalysts supported on some selected sup-

* Corresponding author.
E-mail address: edpark@ajou.ac.kr (E.D. Park).

http://dx.doi.org/10.1016/j.cattod.2016.12.036
0920-5861/

ports such as γ-Al_2O_3, SiO_2, TiO_2, CeO_2, and ZrO_2. Among them, the Ni/CeO_2 catalyst was selected as the best catalyst. Furthermore, we have also found that the methanation activity over Ni/CeO_2 is proportional to the surface area of CeO_2. Since these methanation reactions are exothermic and thermodynamically limited at high temperatures, it is quite desirable to carry out these reactions at low temperatures to achieve high conversions of CO and CO_2. Therefore, a number of series Ni-CeO_2 catalysts containing different Ni contents were prepared by co-precipitation method and applied to CO and CO_2 methanation to find out the optimum Ni content. The stability test was also carried out for the selected catalyst.

2. Experimental

2.1. Preparation of catalysts

Different supports, such as SiO_2 (Zeochem, ZEOprep 60, S_{BET} = 542 m^2/g), TiO_2 (Degussa, P25, S_{BET} = 51 m^2/g), γ-Al_2O_3 (Alfa-aesar, S_{BET} = 162 m^2/g), CeO_2 (Rhodia, HSA20, S_{BET} = 140 m^2/g), and CeO_2 (Rhodia, S_{BET} = 230 m^2/g) were purchased and used as received. Only ZrO_2 (S_{BET} = 50 m^2/g) was prepared by precipitation method from an aqueous solution of $ZrO(NO_3)_2{\cdot}2H_2O$ (Junsei Chemical) and Na_2CO_3 (Junsei Chemical). To change the surface area of ceria, CeO_2 (Rhodia, HSA20, S_{BET} = 140 m^2/g) was calcined in air at 800 and 1000 °C, respectively. To differentiate each ceria support with different surface areas, its surface area is denoted in parenthesis, e.g. CeO_2 (55) implies the ceria support with a surface area of 55 m^2/g, which was prepared through calcination of CeO_2 (Rhodia, HSA20, S_{BET} = 140 m^2/g) at 800 °C.

Various supported Ni catalysts were prepared by wet impregnation. 2.81 g of $Ni(NO_3)_2{\cdot}6H_2O$ (Junsei Chemical) was dissolved into 50 mL of deionized water and mixed with 5 g of support. The excess water was slowly removed using a rotary evaporator (BUCHI, Switzerland). The recovered powder was dried in an oven at 120 °C for 12 h and calcined in an air stream at 500 °C for 3 h. These calcined samples were reduced in a H_2 stream at 500 °C for 1 h before reaction. The Ni content was intended to be 10 wt% for supported Ni catalysts.

$Ni_aCe_{1-a}O_x$ ($0.3 \leq a \leq 0.9$) catalysts were prepared using a co-precipitation method at room temperature. $Ni(NO_3)_2{\cdot}6H_2O$ (Junsei Chemical) and $Ce(NO_3)_3{\cdot}6H_2O$ (Junsei Chemical) were first dissolved in deionized water to make solutions with different mole fractions of Ni. Then, aqueous Na_2CO_3 solution was added dropwise under vigorous stirring to reach a final pH 9 and the slurry was aged for 3 h without stirring at room temperature. The suspension was filtered and washed with deionized water and dried at 110 °C and calcined in air at 500 °C for 5 h. All the prepared catalysts were reduced in hydrogen at 500 °C before reaction.

For comparison, NiO nanoparticles were synthesized as described in the previous work [28]. Briefly, an aqueous $Ni(NO_3)_2{\cdot}6H_2O$ (Junsei Chemical) solution was added dropwise to the poly(ethylene glycol)-*block*-poly (propylene)-*block*-poly(ethylene glycol) (PEG-PPG-PEG, M_n = 8400, Aldrich) mixture in which PEG-PPG-PEG was mixed with NaOH (Samchun Chemical) in deionized water. The resulting mixture was stirred at room temperature for 1 h, centrifuged, washed three times with water and then with isopropanol (Aldrich), and dried at 50 °C for 12 h. The dried powder was calcined at 500 °C for 2 h in an air stream.

2.2. Characterization of catalysts

The specific surface area of the sample was measured on a Micromeritics ASAP 2020 system and calculated by the Brunauer-Emmett-Teller (BET) method. Prior to the measurement, the sample was degassed under vacuum for 6 h at 200 °C.

Powder X-ray diffraction (XRD) experiments were carried out on a Rigaku D/Max instrument with a Cu Kα source. The primary crystallite sizes of the catalysts were determined using the Scherrer equation [29],

$$L = \frac{0.9\lambda_{k\alpha 1}}{B_{(2\theta)}\cos\theta_{\max}}, \quad (3)$$

where L denotes the average particle size, 0.9 is the value in radians when $B_{(2\theta)}$ is the full width at half maximum (FWHM) of the peak, $\lambda_{K\alpha 1}$ is the wavelength of the X-ray radiation (0.15406 nm), and θ_{max} is the angular position at the (111) peak maximum of Ni.

The Ni content was confirmed using inductively coupled plasma-atomic emission spectroscopy (ICP-AES) (Thermo Scientific iCAP 6500).

Hydrogen temperature-programmed reduction (H_2-TPR) of the sample was carried out on a Micromeritics Autochem 2910 equipped with a thermal conductivity detector (TCD). H_2-TPR was performed using 10 mol% H_2/Ar at a flow rate of 30 mL/min in the temperature range 40–900 °C at a heating rate of 10 °C/min. The hydrogen consumption was calculated based on the H_2-TPR patterns of predetermined amount of Ag_2O.

Temperature-programmed desorption (TPD) of the sample was carried out on a Micromeritics Autochem 2910 equipped with a TCD and mass spectrometric detector. A pulsed CO_2 chemisorption was conducted at room temperature by injection of 0.50 mL of 15 mol% CO_2 balanced with He in He stream. TPD was performed using He at a flow rate of 30 mL/min in the temperature range 40–900 °C at a heating rate of 10 °C/min. The ion signals recorded at m/e = 44 was utilized for monitoring desorbed CO_2.

2.3. Catalytic activity test

The catalytic activity tests were conducted at atmospheric pressure using a continuous fixed bed reactor system. Generally, 0.10 g of the catalyst that had been retained between 45 and 80 mesh sieves was loaded into the quartz reactor (internal diameter = 3 mm and length = 345 mm) and brought into contact with a feed composed of 1 mol% CO or CO_2, 50 mol% H_2, and 49 mol% He at a flow rate of 100 mL/min. The mass flow rate of each gas was controlled with a mass flow controller (MFC) (Brooks Instrument). The reaction temperature was measured by a thermocouple placed in the catalyst bed.

In order to obtain the kinetic data for CO and CO_2 methanation, 50 mg of the catalyst was diluted with 0.15 g of α-Al_2O_3 to avoid the generation of hot spot in the catalyst bed. The steady-state activity data at different temperatures were measured only when CO or CO_2 conversion was less than 15%.

The reactants and products were separated using a packed column filled with Carbosphere® and capillary Poraplot Q column, and analyzed using an online gas chromatographer (HP 6890) fitted with a TCD and flame ionization detector. The conversion of CO and CO_2 and carbon yields to CH_4, CO, C_2H_6, and C_3H_8 were calculated using the following equations:

$$\text{CO conversion}\,(\%) = ([\text{CO}]_{in} - [\text{CO}]_{out})/[\text{CO}]_{in} \times 100, \quad (4)$$

$$\text{CO}_2\ \text{conversion}\,(\%) = ([\text{CO}_2]_{in} - \text{CO}_2]_{out})/[\text{CO}_2]_{in} \times 100, \quad (5)$$

$$\text{Carbon yield to CH}_4(\%) = [\text{CH}_4]_{out}/([\text{CO}]_{in} + [\text{CO}_2]_{in}) \times 100, \quad (6)$$

$$\text{Carbon yield to CO}(\%) = [\text{CO}]_{out}/[\text{CO}_2]_{in} \times 100, \quad (7)$$

$$\text{Carbon yield to C}_2\text{H}_6(\%) = (2 \times [\text{C}_2\text{H}_6]_{out})/([\text{CO}]_{in} + [\text{CO}_2]_{in}) \times 100, \quad (8)$$

Please cite this article in press as: T.A. Le, et al., CO and CO_2 methanation over supported Ni catalysts, Catal. Today (2016), http://dx.doi.org/10.1016/j.cattod.2016.12.036

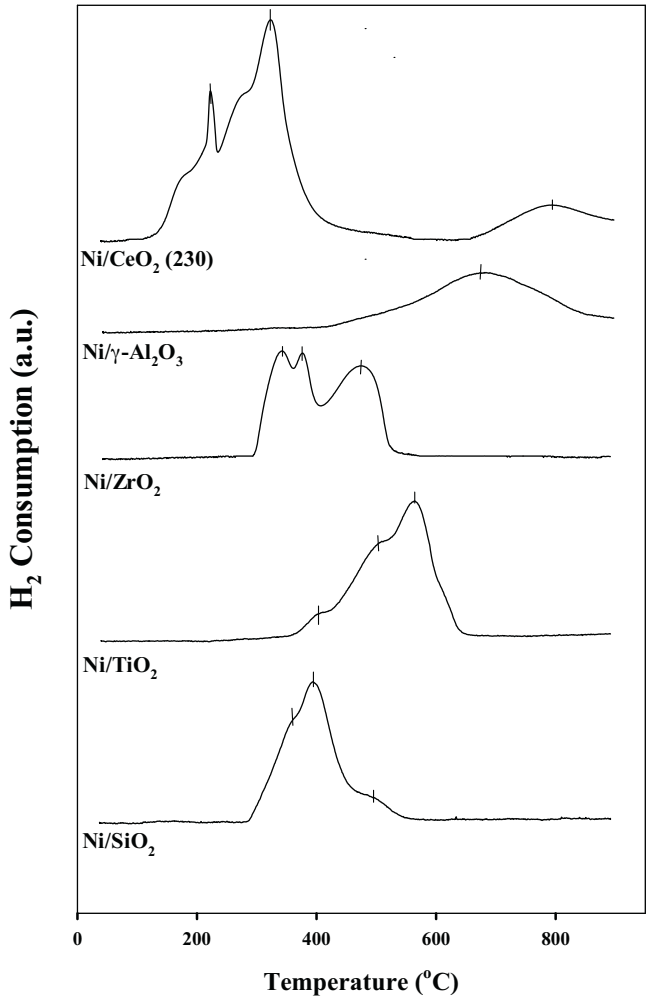

Fig. 1. H_2-TPR profiles of supported Ni catalysts.

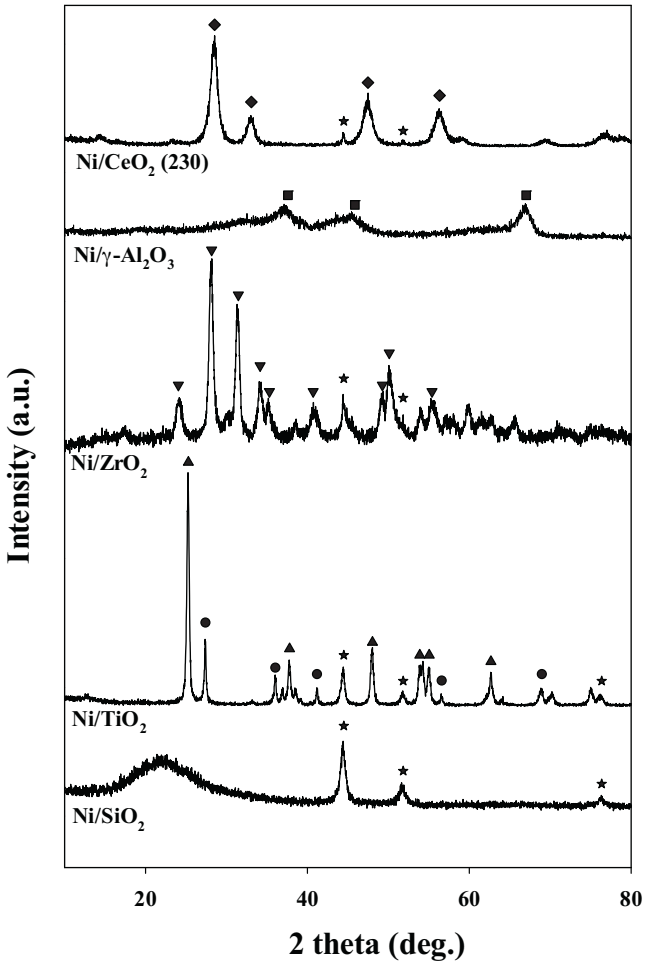

Fig. 2. X-ray diffraction patterns of supported Ni catalysts reduced at 500 °C. (▲) Anatase, JCPDS 21-1272, (●) Rutile, JCPDS 21-1276, (▼) ZrO_2, JCPDS 37-1484, (■) γ-Al_2O_3, JCPDS 10-0425, (♦) CeO_2, JCPDS 43-1002, (★) Ni, JCPDS 04-0850.

$$\text{Carbon yield to } C_3H_8(\%) = (3 \times [C_3H_8]_{out})/([CO]_{in} + [CO_2]_{in}) \times 100, \quad (9)$$

where $[CO]_{in}$ and $[CO_2]_{in}$ represent the concentration of CO and CO_2 in the feed stream and $[CO]_{out}$, $[CO_2]_{out}$, $[CH_4]_{out}$, $[C_2H_6]_{out}$, and $[C_3H_8]_{out}$ denote the concentration of CO, CH_4, C_2H_6, and C_3H_8 in the output stream, respectively. The difference between CO or CO_2 conversion and total carbon yield in all experiments is within an experimental error.

3. Results and discussion

3.1. Supported Ni catalysts prepared by wet impregnation

The physical properties of Ni catalysts supported on different supports such as γ-Al_2O_3, SiO_2, TiO_2, CeO_2, and ZrO_2 are presented in Table 1. The BET surface area of each supported Ni catalyst was lower than that of the support itself. This can be explained by the pore filling in the catalyst preparation step. The ratio of reduction in the BET surface area after an impregnation of Ni was significant for the Ni catalysts supported on the supports with high surface areas and small average pore diameters.

To find out the reducibility of nickel oxide species on different supports, H_2-TPR patterns were obtained for supported Ni catalysts calcined in air at 500 °C, as shown in Fig. 1. It is worth noting that the lowest TPR peak can be found over Ni/CeO_2. It is generally accepted that the smaller metal oxide particle can be reduced at a lower temperature than the larger ones as long as the interaction between a metal oxide particle and a support can be neglected. Therefore, it can be said that the smallest NiO nanoparticles are formed on ceria support, which results in the formation of the smallest Ni particles after reduction. This is consistent with the XRD patterns of Ni/CeO_2 reduced at 500 °C in which very weak XRD peaks corresponding to the metallic Ni were observed (Fig. 2). In the case of Ni/γ-Al_2O_3, no XRD peak representing the metallic Ni can be obtained. This can be explained that most Ni oxides on γ-Al_2O_3 were not reduced at 500 °C based on its H_2-TPR patterns where the main peak was observed at 678 °C. It can be conclude that there exists a strong interaction between NiO and γ-Al_2O_3 surface. Based on the H_2-TPR patterns, the interaction between NiO and TiO_2 surface seems to be weaker than that between NiO and γ-Al_2O_3 surface but much stronger than those between NiO and other supports such as CeO_2, SiO_2, and ZrO_2. The amount of hydrogen consumed during H_2-TPR experiments were calculated and listed in Table 1. It is worth noting that the amount of consumed hydrogen was larger for the Ni catalysts supported on reducible metal oxides such as CeO_2, TiO_2, and ZrO_2 than for the ones supported on irreducible metal oxides such as γ-Al_2O_3 and SiO_2. Especially, the amount of consumed hydrogen was the largest for Ni/CeO_2 even though the high-temperature TPR peak centered at 795 °C due to the reduction of bulk CeO_2 was not

Please cite this article in press as: T.A. Le, et al., CO and CO_2 methanation over supported Ni catalysts, Catal. Today (2016), http://dx.doi.org/10.1016/j.cattod.2016.12.036

Table 1
Physicochemical properties of supported Ni catalysts.

Catalyst	S_{BET} (m^2/g)	Pore volume (cm^3/g)	Average pore diameter (nm)[a]	Crystallite size of Ni (nm)[b]	H_2 consumption (mmol H_2/g)[c]
Ni/CeO_2 (230)	117	0.13	4.4	n.d.	2.4
Ni/ZrO_2	36	0.11	11.8	12	1.5
Ni/SiO_2	380	0.58	6.1	11	1.2
Ni/TiO_2	31	0.26	32.8	17	1.5
$Ni/\gamma\text{-}Al_2O_3$	130	0.22	7.4	n.d.	1.2

[a] Average pore diameter was determined by BJH model.
[b] Crystallite size of Ni was determined by Scherrer formula for supported Ni catalysts reduced at 500 °C.
[c] H_2 consumption was determined based on the H_2-TPR.

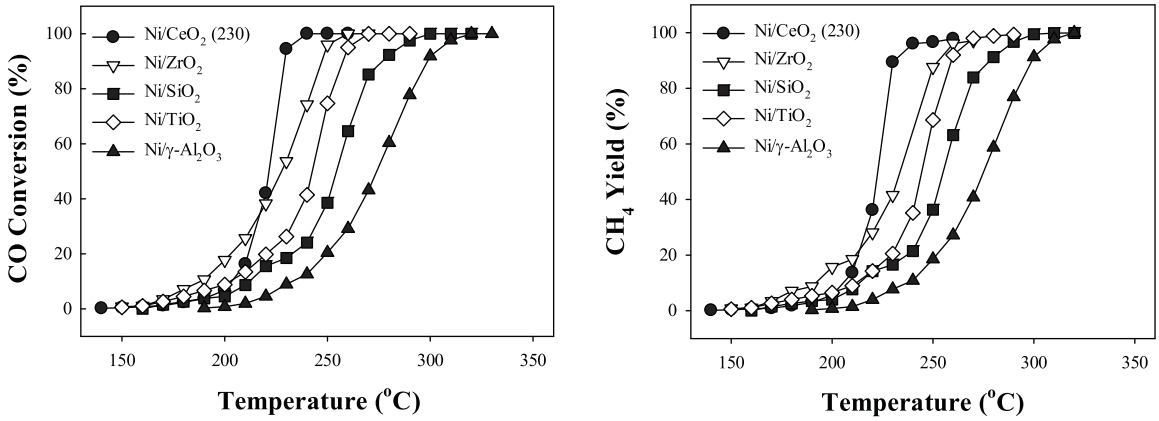

Fig. 3. Catalytic performance of supported Ni catalysts for CO methanation. Reaction conditions: 1 mol% CO, 50 mol% H_2, 49 mol% He, F/W = 1000 mL/min/$g_{cat.}$

considered. This also supports that there exists a strong interaction between Ni and ceria support.

The catalytic performance for CO and CO_2 methanation was evaluated over Ni catalysts supported on different supports. Fig. 3 shows that the temperature achieving 100% CO conversion increased in the following order: $Ni/CeO_2 < Ni/ZrO_2 < Ni/TiO_2 < Ni/SiO_2 < Ni/\gamma\text{-}Al_2O_3$. The highest catalytic activity of Ni/CeO_2 can be ascribed to the smallest Ni particle size. On the other hand, the lowest catalytic activity of $Ni/\gamma\text{-}Al_2O_3$ must be due to the incomplete reduction of Ni oxides under present reductive pretreatment conditions. Besides Ni dispersion, the support effect cannot be neglected because Ni/ZrO_2 and Ni/TiO_2 which have large Ni particles exhibit the higher catalytic activity compared with Ni/SiO_2 with small Ni particles. Methane was determined to be a major product irrespective of supports for all reaction temperatures. Besides methane, ethane and propane were also detected at low temperatures (Fig. S1). The carbon yields to ethane and propane appear to be dependent on the support. High carbon yields to ethane and propane were observed over Ni/ZrO_2. Fig. 4 exhibits that the temperature achieving 100% CO_2 conversion increased in the following order: $Ni/CeO_2 < Ni/SiO_2 < Ni/ZrO_2 < Ni/TiO_2 \sim Ni/\gamma\text{-}Al_2O_3$. This seems to be closely related to the Ni dispersion as long as the Ni species are fully reduced. Methane was a predominant product during CO_2 methanation. The formation of ethane was observed only over Ni/CeO_2 and only CO was detected as a byproduct over the other supported Ni catalysts (Fig. S2). The activation energy for CO methanation of $Ni/\gamma\text{-}Al_2O_3$, Ni/SiO_2, Ni/TiO_2, Ni/CeO_2, and Ni/ZrO_2 was determined to be 153, 100, 90, 115, and 87 kJ/mol, respectively, based on the Arrhenius plot (Fig. S3). These values are similar with those in the previous reports [23]. Note that the activation energy of $Ni/\gamma\text{-}Al_2O_3$, in which most Ni oxides were not reduced, is much higher than those of other catalysts.

The amount of CO_2 chemisorbed at room temperature was determined to be 232, 39, 9, 3, 1 μmol $CO_2/g_{cat.}$ for Ni/CeO_2, Ni/ZrO_2, $Ni/\gamma\text{-}Al_2O_3$, Ni/TiO_2, and Ni/SiO_2, respectively. The CO_2-TPD patterns were obtained as shown in Fig. 5. All the catalysts except for Ni/CeO_2 has only weak low-temperature TPD peak, which implies that there exist only weak basic sites for CO_2 chemisorption. On the other hand, a rather broad and strong TPD peak was also observed around 500 °C over Ni/CeO_2. This strong CO_2 chemisorption might have a beneficial effect on the catalytic activity for CO_2 methanation.

Since ceria was selected as the best support for these reactions, a further work was carried out to find out the effect of surface area of ceria on the catalytic activities. H_2-TPR patterns were obtained for Ni/CeO_2 catalyst with different surface areas, as shown in Fig. 6. The H_2-TPR patterns can be separated into three different parts. A first weak TPR peak is found around 220 °C with a rather broad shoulder at lower temperatures. This might be due to the reduction of very small NiO particles weakly interacting with ceria. The second sharp TPR peak is observed around 320 °C. This is owing to the reduction of NiO particles and surface ceria. The surface ceria can be reduced easily by hydrogen dissociated on the metallic Ni. The high-temperature TPR peak is ascribed to the reduction of bulk ceria. Fig. S4 clearly shows that the peak intensity of the first TPR peak decreased with decreasing surface area of the support. This can be interpreted that the number of very small NiO particles decreases with decreasing surface area of the support. Fig. 7 reveals that the intensity of the XRD peaks was strengthened with decreasing surface area of the support. The crystallite sizes of ceria and Ni were calculated to be increased with decreasing surface area of the support, as shown in Table 2.

The catalytic performance for CO and CO_2 methanation was evaluated over Ni/CeO_2 catalysts with different surface areas. Figs. 8 and 9 show that the catalytic activities for both reactions increased with increasing surface area of the support. Methane is

Please cite this article in press as: T.A. Le, et al., CO and CO_2 methanation over supported Ni catalysts, Catal. Today (2016), http://dx.doi.org/10.1016/j.cattod.2016.12.036

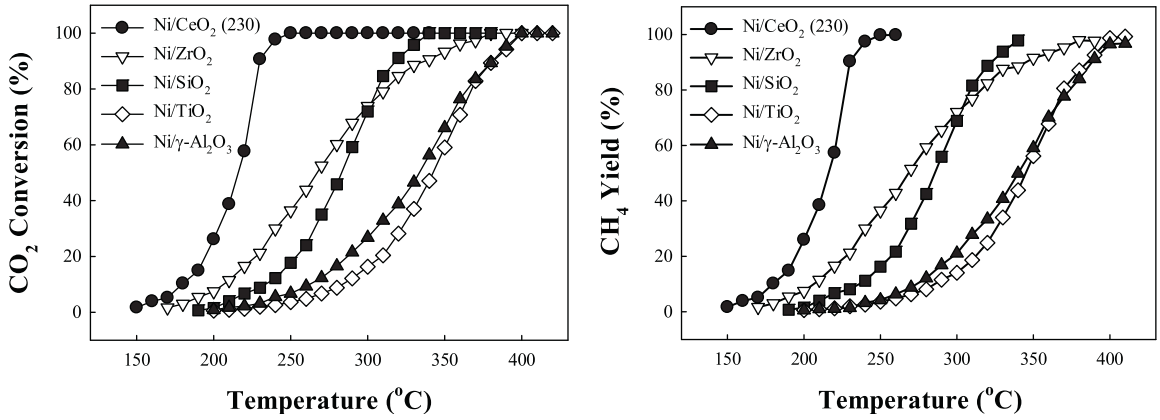

Fig. 4. Catalytic performance of supported Ni catalysts for CO_2 methanation. Reaction conditions: 1 mol% CO_2, 50 mol% H_2, 49 mol% He, F/W = 1000 mL/min/$g_{cat.}$

Table 2
Physicochemical properties of Ni/CeO_2 catalysts with different surface areas.

Catalyst	S_{BET} (m^2/g)	Pore volume (cm^3/g)	Average pore diameter (nm)[a]	Crystallite size (nm)[b]		H_2 consumption (mmol H_2/g)[c]
				CeO_2	Ni	
Ni/CeO_2 (230)	117	0.13	4.4	9	n.d.	2.4
Ni/CeO_2 (140)	94	0.22	9.3	8	9	2.5
Ni/CeO_2 (55)	44	0.22	20.1	18	21	2.3
Ni/CeO_2 (19)	15	0.15	39.9	37	27	2.2

[a] Average pore diameter was determined by BJH model.
[b] Crystallite size of Ni was determined by Scherrer formula for supported Ni catalysts reduced at 500 °C.
[c] H_2 consumption was determined based on the H_2-TPR.

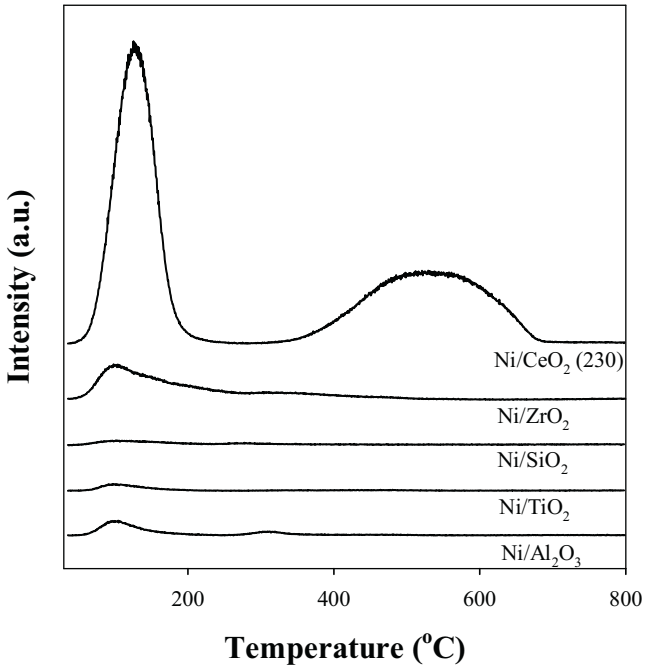

Fig. 5. CO_2-TPD profiles of supported Ni catalysts.

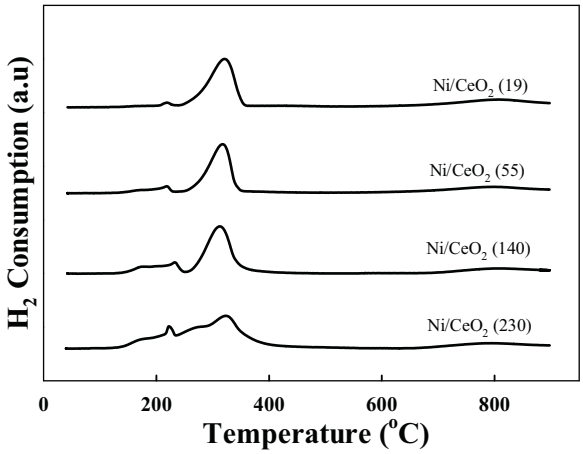

Fig. 6. H_2-TPR profiles of Ni/CeO_2 with different surface areas.

the major product for both CO and CO_2 methanation. In the case of CO methanation, ethane and propane were also observed as byproducts (Fig. S5). On the other hand, the formation of propane was not detected for CO_2 methanation (Fig. S6). CO formation was confirmed over Ni/CeO_2 (19) which had the lowest catalytic activity. Therefore, it can be concluded that the Ni dispersion is a critical factor to control the catalytic activity for Ni/CeO_2 catalysts.

3.2. *Ni-CeO_2 catalysts prepared by co-precipitation*

Various Ni-CeO_2 catalysts with different Ni contents were prepared by co-precipitation method to increase the specific catalytic activity. The physical properties of a series of Ni-CeO_2 catalysts are listed in Table 3. The BET surface areas of Ni-CeO_2 catalysts were larger than that of unsupported NiO catalysts. However, there was no correlation between the BET surface area and the Ni content for Ni-CeO_2 catalysts. On the other hand, the pore volume and average pore diameter increased with increasing Ni content.

H_2-TPR patterns were obtained for Ni-CeO_2 catalysts calcined in air at 500 °C to find out the reducibility of nickel oxide species, as shown in Fig. 10. For comparison, H_2-TPR pattern of unsupported NiO is also displayed. The main TPR peak is shifted to a higher temperature with increasing Ni content for Ni-CeO_2 catalysts. Compared with H_2-TPR patterns of Ni/CeO_2 catalysts, TPR

Please cite this article in press as: T.A. Le, et al., CO and CO_2 methanation over supported Ni catalysts, Catal. Today (2016), http://dx.doi.org/10.1016/j.cattod.2016.12.036

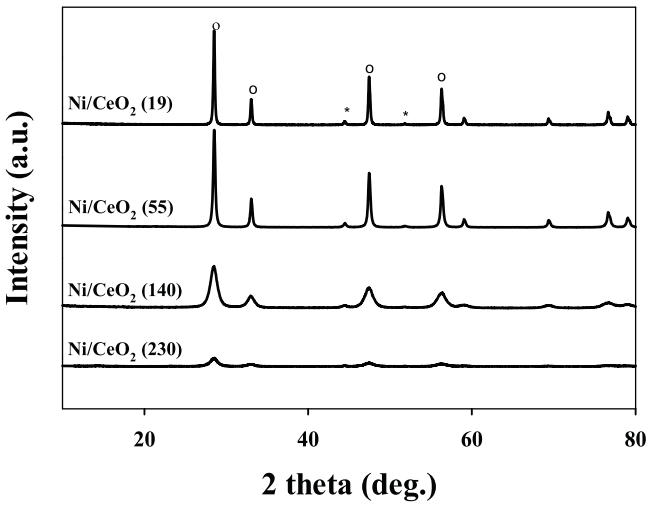

Fig. 7. X-ray diffraction patterns of Ni/CeO_2 catalysts with different surface areas reduced at 500 °C. (○) CeO_2, JCPDS 43–1002, (*) Ni, JCPDS 04-0850.

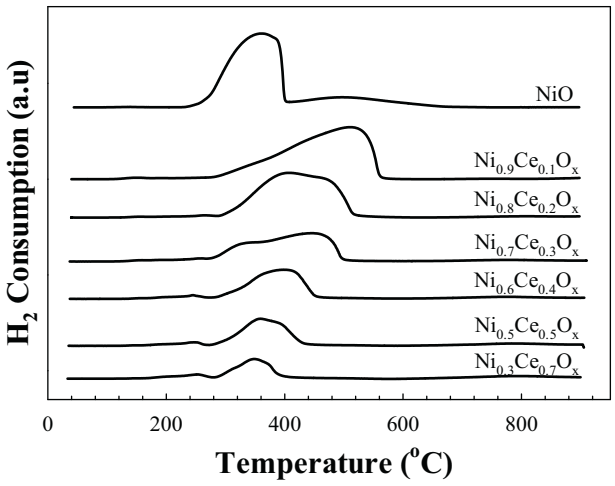

Fig. 10. H_2-TPR profiles of NiO and $Ni-CeO_2$ catalysts with different Ni contents.

peaks were observed at higher temperatures for $Ni-CeO_2$ catalysts, which implies that there exists a stronger interaction between NiO and ceria in $Ni-CeO_2$ catalysts than in Ni/CeO_2 ones. The amount of consumed hydrogen during H_2-TPR experiment increased with increasing Ni content (Table 3).

X-ray diffraction patterns were obtained for $Ni-CeO_2$ catalysts reduced at 500 °C (Fig. S7). The crystallite size of Ni was calculated and listed in Table 3. It decreased with increasing Ni content, reached the minimum value for $Ni_{0.7}Ce_{0.3}O_x$ and $Ni_{0.8}Ce_{0.2}O_x$, and increased with further increasing Ni contents.

The catalytic performance for CO and CO_2 methanation was evaluated over $Ni-CeO_2$ and unsupported Ni catalysts. As shown in Figs. 11 and 12, the $Ni-CeO_2$ catalysts were superior to unsupported Ni catalysts in all cases. The highest catalytic activity was obtained over $Ni_{0.8}Ce_{0.2}O_x$ catalyst for both reactions. Methane was determined to be a major product for both reactions. Besides methane, ethane and propane were also detected at low temperatures for CO

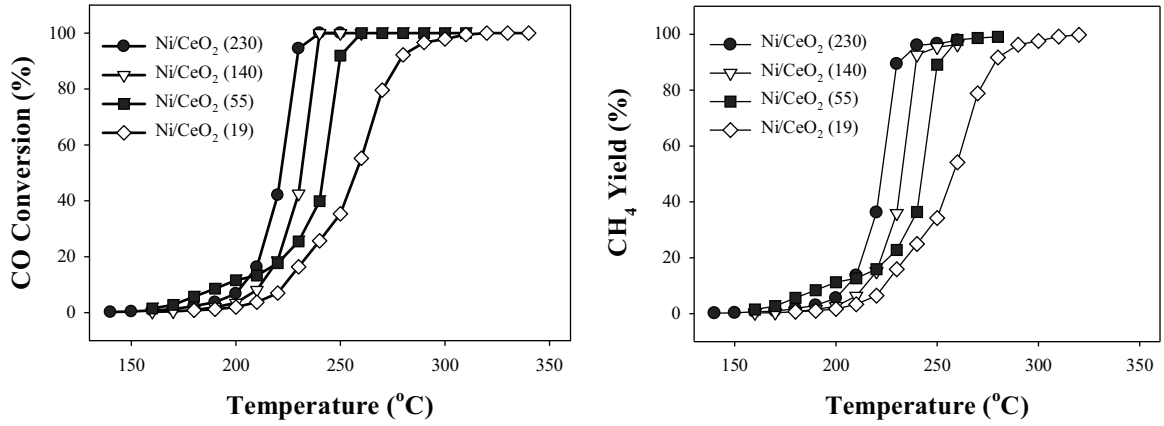

Fig. 8. Catalytic performance of Ni/CeO_2 with different surface areas for CO methanation. Reaction conditions: 1 mol% CO, 50 mol% H_2, 49 mol% He, F/W = 1000 mL/min/$g_{cat.}$

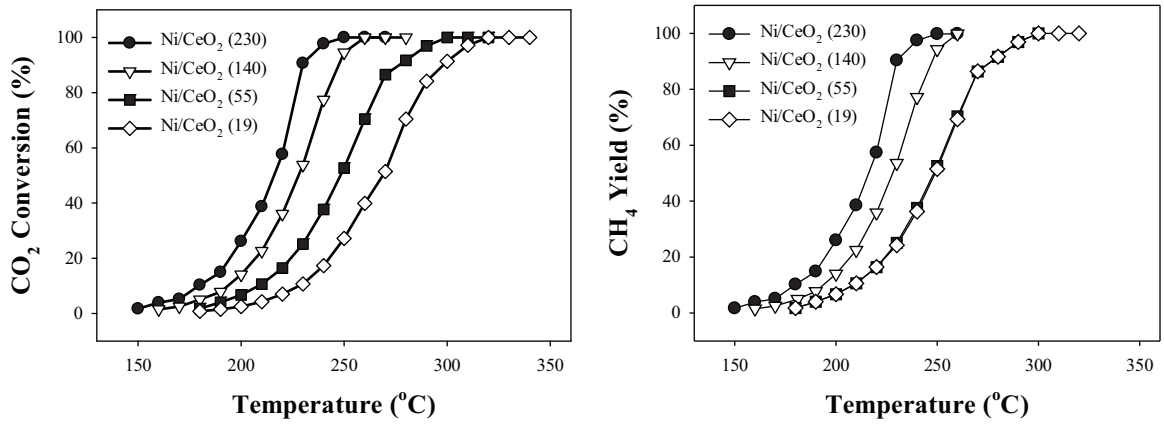

Fig. 9. Catalytic performance of Ni/CeO_2 with different surface areas for CO_2 methanation. Reaction conditions: 1 mol% CO_2, 50 mol% H_2, 49 mol% He, F/W = 1000 mL/min/$g_{cat.}$

Please cite this article in press as: T.A. Le, et al., CO and CO_2 methanation over supported Ni catalysts, Catal. Today (2016), http://dx.doi.org/10.1016/j.cattod.2016.12.036

Table 3
Physicochemical properties of Ni-CeO_2 catalysts with different Ni contents.

Catalyst	S_{BET} (m^2/g)	Pore volume (cm^3/g)	Average pore diameter (nm)[a]	Crystallite size of Ni (nm)[b]	H_2 consumption (mmol H_2/g)[c]
NiO	22	0.18	32.8	33	13
$Ni_{0.3}Ce_{0.7}O_x$ (wt.%)	91	0.09	5.5	n.d.	1.5
$Ni_{0.5}Ce_{0.5}O_x$ (25 wt.%)	83	0.17	8.9	32	4.4
$Ni_{0.6}Ce_{0.4}O_x$ (34 wt.%)	89	0.22	11.5	22	5.6
$Ni_{0.7}Ce_{0.3}O_x$ (44 wt.%)	73	0.33	19.8	12	7.9
$Ni_{0.8}Ce_{0.2}O_x$ (58 wt.%)	64	0.42	21.5	12	10
$Ni_{0.9}Ce_{0.1}O_x$ (75 wt.%)	76	0.44	22.5	16	13

[a] Average pore diameter was determined by BJH model.
[b] Crystallite size of Ni was determined by Scherrer formula for Ni-CeO_2 catalysts reduced at 500 °C.
[c] H_2 consumption was determined based on the H_2-TPR.

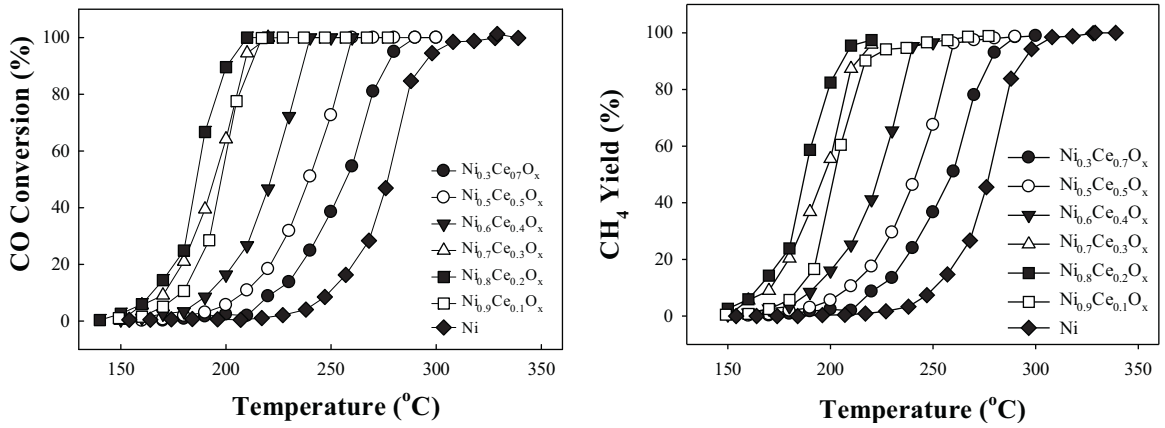

Fig. 11. Catalytic performance of Ni-CeO_2 catalysts with different Ni contents for CO methanation. Reaction conditions: 1 mol% CO, 50 mol% H_2, 49 mol% He, F/W = 1000 mL/min/$g_{cat.}$

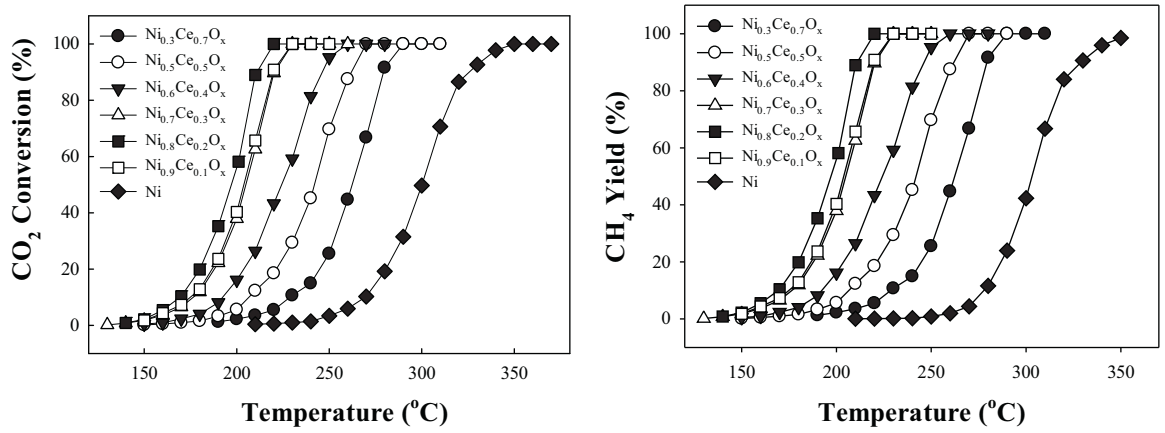

Fig. 12. Catalytic performance of Ni-CeO_2 catalysts with different Ni contents for CO_2 methanation. Reaction conditions: 1 mol% CO_2, 50 mol% H_2, 49 mol% He, F/W = 1000 mL/min/$g_{cat.}$

methanation (Fig. S8). However, only ethane was observed for CO_2 methanation (Fig. S9).

Compared with Ni-based catalysts reported previously, the $Ni_{0.8}Ce_{0.2}O_x$ catalyst can be classified into most active catalyst group for CO methanation (Fig. S10). Its activation energy is determined to be 133 kJ/mol, which is slightly higher than that of Ni/CeO_2 catalysts. On the other hand, the activation energy for CO_2 methanation was calculated to be 95 kJ/mol.

Since CO and CO_2 methanation are highly exothermic reactions, the thermal stability was checked for the best catalyst. The catalytic activities for CO and CO_2 methanation of $Ni_{0.8}Ce_{0.2}O_x$ catalyst after a reaction at 400 or 500 °C for 24 h were compared with those of the fresh $Ni_{0.8}Ce_{0.2}O_x$ catalyst (Figs. S11 and S12). The catalytic activity appeared to be decreased slightly after a reaction at high temperatures. The crystalline sizes of Ni of the catalyst after a reaction at 400 and 500 °C for 24 h were determined to be 16 and 19 nm,

Please cite this article in press as: T.A. Le, et al., CO and CO_2 methanation over supported Ni catalysts, Catal. Today (2016), http://dx.doi.org/10.1016/j.cattod.2016.12.036

respectively. The crystalline sizes of CeO_2 of the catalyst after a reaction at 400 and 500 °C for 24 h were also estimated to be 9 and 12 nm, respectively. This increase in the crystalline size of Ni and CeO_2 is responsible for the decreased catalytic activity for CO and CO_2 methanation after reaction at high temperatures. Owing to the thermodynamic limitations for CO and CO_2 methanation, it is quite plausible to carry out these reactions at low temperatures to achieve high conversions of CO and CO_2. Therefore, this highly active $Ni_{0.8}Ce_{0.2}O_x$ catalyst can be installed in the first methanation reactor in a series of adiabatic reactors with inter-stage coolers to initiate reaction at low temperatures. This catalyst can be also applied to a low-temperature methanation reactor in which the reaction temperature is well controlled not to cause catalyst sintering and low single-pass conversions of CO or CO_2 due to the thermodynamic limitation.

4. Conclusion

Ni/CeO_2 was determined to be the most active for CO and CO_2 methanation among Ni catalysts supported on different supports such as γ-Al_2O_3, SiO_2, TiO_2, CeO_2, and ZrO_2. These catalytic activities increased with increasing surface area of CeO_2. The high Ni dispersion and an intimate contact between Ni and ceria appeared to be responsible for the high catalytic activity for CO methanation. Furthermore, strong CO_2 adsorption on CeO_2 is beneficial for CO_2 methanation. A further increase in the specific catalytic activity for CO and CO_2 methanation can be made using Ni-CeO_2 catalyst prepared by co-precipitation method. The best catalyst, $Ni_{0.8}Ce_{0.2}O_x$, has the high Ni content and small Ni particles. This catalyst can be applied to the low-temperature CO or CO_2 methanation reactor to achieve high single-pass conversions of CO and CO_2.

Acknowledgments

This work was supported by the New & Renewable Energy Core Technology Program (20123010040010) and Human Resources Program in Energy Technology (No. 20154010200820) of the Korea Institute of Energy Technology Evaluation and Planning (KETEP), granted financial resource from the Ministry of Trade, Industry & Energy, Republic of Korea. This work was also supported by C1 Gas Refinery Program through the National Research Foundation of Korea (NRF) funded by the Ministry of Science, ICT & Future Planning (2015M3D3A1A01064899).

Appendix A. Supplementary data

Supplementary data associated with this article can be found, in the online version, at http://dx.doi.org/10.1016/j.cattod.2016.12.036.

References

[1] M.V. Twigg (Ed.), Catalyst Handbook, 2nd ed., Manson Publishing, London, 1996.
[2] E.D. Park, D. Lee, H.C. Lee, Catal. Today 139 (2009) 280.
[3] W. Wang, S. Wang, X. Ma, J. Gong, Chem. Soc. Rev 40 (2011) 3703.
[4] H. Ban, C. Li, Y. Zhang, F. Meng, H. Zheng, Z. Li, Rev. Adv. Sci. Eng. 4 (2015) 126.
[5] M. Götz, J. Lefebvre, F. Mörs, A.M. Koch, F. Graf, S. Bajohr, R. Reimert, T. Kolb, Renew. Energy 85 (2016) 1371.
[6] P. Sabatier, J.B. Senderens, C.R. Acad. Sci. Paris 134 (1902) 514.
[7] M.A. Vannice, J. Catal 37 (1975) 448.
[8] B. Mao, S.S.K. Ma, X. Wang, H. Su, S.H. Chan, Catal. Sci. Technol. 6 (2016) 4048.
[9] M.A.A. Aziz, A.A. Jalil, S. Triwahyono, A. Ahmad, Green Chem. 17 (2015) 2647.
[10] J. Gao, Q. Liu, F. Gu, B. Liu, Z. Zhong, F. Su, RSC Adv. 5 (2015) 22759.
[11] S. Rönsch, J. Schneider, S. Matthischke, M. Schlüter, M. Götz, J. Lefebvre, P. Prabhakaran, S. Bajohr, Fuel 166 (2016) 276.
[12] X. Su, J. Xu, B. Liang, H. Duan, B. Hou, Y. Huang, J. Energy Chem. 25 (4) (2016) 553.
[13] S. Takenaka, T. Shimizu, K. Otsuka, Int. J. Hydrogen Energy 29 (2004) 1065.
[14] J. Gao, C. Jia, J. Li, F. Gu, G. Xu, Z. Zhong, F. Su, Ind. Eng. Chem. Res. 51 (31) (2012) 10345.
[15] M.A.A. Aziz, A.A. Jalil, S. Triwahyono, R.R. Mukti, Y.H. Taufiq-Yap, M.R. Sazegar, Appl. Catal. B 147 (2014) 359.
[16] Y. Yu, G.-Q. Jin, Y.-Y. Wang, X.-Y. Guo, Fuel Process. Technol. 92 (12) (2011) 2293.
[17] A. Borgschulte, N. Gallandat, B. Probst, R. Suter, E. Callini, D. Ferri, Y. Arroyo, R. Erni, H. Geerlings, A. Zuttel, Phys. Chem. Chem. Phys. 15 (2013) 9620.
[18] C. Jia, J. Gao, J. Li, F. Gu, G. Xu, Z. Zhong, F. Su, Catal. Sci. Technol. 3 (2) (2013) 490.
[19] S. Tada, T. Shimizu, H. Kameyama, T. Haneda, R. Kikuchi, Int. J. Hydrogen Energy 37 (7) (2012) 5527.
[20] M.M. Zyryanova, P.V. Snytnikov, R.V. Gulyaev, Yu.I. Amosov, A.I. Boronin, V.A. Sobyanin, Chem. Eng. J. 238 (2014) 189.
[21] B. Nematollahi, M. Rezaei, E. Nemati Lay, Int. J. Hydrogen Energy 40 (2015) 8539.
[22] M.V. Konishcheva, D.I. Potemkin, P.V. Snytnikov, M.M. Zyryanova, V.P. Pakharukova, P.A. Simonov, V.A. Sobyanin, Int. J. Hydrogen Energy 40 (2015) 14058.
[23] B. Nematollahi, M. Rezaei, E. Nemati Lay, J. Rare Earth 33 (2015) 619–628.
[24] E. Rombi, M.G. Cutrufello, L. Atzori, R. Monaci, A. Ardu, D. Gazzoli, P. Deiana, I. Ferinoa, Appl. Catal. A 515 (2016) 144.
[25] F. Ocampo, B. Louis, L. Kiwi-Minsker, A.-C. Roger, Appl. Catal. A 392 (2011) 36.
[26] W. Zhen, B. Li, G. Lu, J. Ma, Chem. Commun. 51 (2015) 1728.
[27] W. Zhang, Q. Ge, H. Xu, Sci. Adv. Mater. 3 (6) (2011) 1046.
[28] P. Lakshmanan, M.S. Kim, E.D. Park, Appl. Catal. A 513 (2016) 98.
[29] A. Patterson, Phys. Rev. 56 (10) (1939) 978.

Please cite this article in press as: T.A. Le, et al., CO and CO_2 methanation over supported Ni catalysts, Catal. Today (2016), http://dx.doi.org/10.1016/j.cattod.2016.12.036